Empirical potential-energy function for calcium solids and clusters

Klas M. Andersson, Roy L. Johnston, and John N. Murrell
School of Chemistry and Molecular Sciences, University of Sussex, Falmer, Brighton BN1 9QJ, United Kingdom
(Received 2 August 1993)

An empirical potential-energy function, consisting of two- and three-body terms, has been derived for the study of calcium solids and clusters. With a single set of parameters, this potential reproduces the phonon frequencies and elastic constants of both the low-temperature fcc and the high-temperature bcc crystalline phases to a high degree of accuracy. It also gives a sensible energy profile for the tetragonal (Bain path) interconversion of the two structures, which are both minima along the path. The potential predicts that the fcc and hcp solids have almost equal cohesive energies, with that of the bcc phase being 0.02 eV lower. Other cubic phases and various two-dimensional and one-dimensional structures have lower cohesive energies. The potential leads to the conclusion that the most stable clusters tend to be polytetrahedral, leading to icosahedral packing, thereby maximizing coordination number.

I. INTRODUCTION

The group II metals (Be-Ba) possess fcc, hcp, or bcc crystal structures depending on temperature and pressure.[1] For a given set of conditions $\{P,T\}$, the most stable phase is the one having the lowest chemical potential, but to calculate this we must have an expression for the potential energy of the crystal which can be used to calculate the phonon-dispersion curves and the density of phonon states. The group II metals therefore constitute a valuable testing ground for empirical potentials which are intended to describe the structures and dynamics of a number of solid phases with a single set of parameters.

The objective of the work described in this paper is to derive a potential for calcium which simultaneously gives a good description of the lattice dynamics of the fcc and bcc allotropes. At atmospheric pressure, the low-temperature fcc phase of Ca transforms to bcc at 721 K,[2] while at room temperature this transition occurs at an applied pressure of 19.5 GPa.[3] It is essential that such a potential should have no obvious deficiencies when applied to other three-, two-, and one-dimensional (3D, 2D, 1D) infinite structures or to Ca_n clusters; it should not, for example, make any structure more stable than the fcc lattice.

We select Ca from the group II metals because phonon-dispersion curves and elastic constants have been measured (or derived) for both the fcc (at 300 K) (Ref. 4) and bcc (at 726 K) (Ref. 5) phases, these temperatures being sufficiently close that anharmonic effects (which are reflected in temperature-dependent lattice parameters) will be small. For some time it was thought that Ca also had an hcp phase (the room-temperature structure for Be and Mg) but this is now known to be induced by impurities (probably hydrogen).[1] However, one can be confident from the pattern of temperature- and pressure-induced phase transitions observed in this group,[1,6] that there will be little difference between the fcc and hcp lattice energies.

II. THE POTENTIAL

The type of potential function that we have employed in our treatment of Ca has two-body and three-body terms.[7,8] and has previously been applied to a variety of metallic[9–12] and nonmetallic[13–15] elemental solids and clusters. Further details on the potential and expressions for obtaining force constants (and subsequently elastic constants and phonon frequencies) from the potential can be found in previous papers.[7–9] The potential is defined as the sum of the following contributions:

$$V_{ij}^{(2)}=-D(1+a_2\rho_{ij})\exp(-a_2\rho_{ij}) , \tag{1}$$

$$V_{ijk}^{(3)}=D\times P(Q_1,Q_2,Q_3)\exp(-a_3Q_1) , \tag{2}$$

where

$$\begin{bmatrix}Q_1\\Q_2\\Q_3\end{bmatrix}=\begin{bmatrix}\sqrt{\frac{1}{3}} & \sqrt{\frac{1}{3}} & \sqrt{\frac{1}{3}}\\ 0 & \sqrt{\frac{1}{2}} & -\sqrt{\frac{1}{2}}\\ \sqrt{\frac{2}{3}} & -\sqrt{\frac{1}{6}} & -\sqrt{\frac{1}{6}}\end{bmatrix}\begin{bmatrix}\rho_{ij}\\\rho_{ik}\\\rho_{jk}\end{bmatrix} \tag{3}$$

and

$$\rho_{ij}=(r_{ij}-r_e)/r_e \tag{4}$$

with r_{ij} being the distance between atoms i and j. During optimization a "hard wall" term is added to (1) to prevent collapse of the lattice for certain sets of coefficients that may be explored during the optimization procedure; the hard wall is not included in the final potential. The function P is a polynomial in the symmetry coordinates Q_i, and both cubic and quartic polynomials have been investigated. The totally symmetric quartic polynomial is given by

$$P(Q_1,Q_2,Q_3)=c_0+c_1Q_1+c_2Q_1^2+c_3(Q_2^2+Q_3^2)+c_4Q_1^3+c_5Q_1(Q_2^2+Q_3^2)+c_6(Q_3^3-3Q_3Q_2^2)+c_7Q_1^4$$
$$+c_8Q_1^2(Q_2^2+Q_3^2)+c_9(Q_2^2+Q_3^2)^2+c_{10}Q_1(Q_3^3-3Q_3Q_2^2) . \tag{5}$$

0163-1829/94/49(5)/3089(9)/$06.00

The coefficients of this polynomial are optimized to experimental data for selected values of a_2 and a_3 by a least-squares routine and the best potential (specified by a_2, a_3, and c_0-c_{10}) is selected on the basis of the sum of squared deviations and other criteria; this procedure will be discussed more fully later. D and r_e are scaling factors which ensure that the lattice (or cohesive) energy and lattice spacing of the reference structure (e.g., fcc) are reproduced exactly.

III. DATA USED IN POTENTIAL OPTIMIZATION

Phonon-dispersion curves for fcc Ca have been determined by Stassis *et al.*, by single-crystal inelastic neutron scattering at 300 K.[4] Their tabulated phonon frequencies, at selected points along the high-symmetry (reciprocal space) **q** vectors $[q00]$, $[qq0]$, and $[qqq]$, have been used as input to the least-squares routine (14 frequencies in all). Phonon frequencies are squared, multiplied by the atomic mass and divided by the lattice constant to give a quantity with the same dimensions as the elastic constants, which have also been determined by Stassis *et al.*, using force constants obtained from an eighth-neighbor Born-von Karman (BvK) fit to the phonon-dispersion curves. There are independent elastic constants for fcc Ca which have been determined by Heiroth *et al.*, from polycrystalline neutron data[5] combined with the measured bulk modulus $[B_0=\frac{1}{3}(C_{11}+2C_{12})=0.183\times10^{12}$ dyn cm^{-2}],[16] but for consistency with the phonon frequency data we have used the values calculated by Stassis *et al.*, in our optimization.

It was shown in an earlier paper[11] that the vacancy-formation energy is an important quantity in determining the balance between two-body and three-body terms in the potential. To our knowledge, there has been no experimental determination of the vacancy-formation energy for Ca, so we have taken a value of 0.5 eV, roughly the arithmetic mean of the experimental[17] values for K (0.39 eV) and Al (0.66 eV). Recent calculations by Ghorai give a value of 0.33 eV for the vacancy-formation energy of Ca,[18] but since this is the energy required to form a relaxed vacancy, we believe we are justified in taking the slightly higher value of 0.5 eV. Taking the phonon and elastic constant data in units of 10^{12} dyn cm^2 and the vacancy energy in eV, gives 18 pieces of data, all in the range 0–1, which are given equal weighting in the least squares procedure. The data for fcc Ca are summarized in Table I.

The phonon-dispersion curves of bcc Ca have been determined, by Heiroth *et al.*, using force constants derived from a third-neighbor axially-symmetric BvK fit to their polycrystalline neutron time-of-flight spectra (measured at 726 K).[5] We have measured selected frequencies from the published curves and treated them in an analogous manner to that described above for fcc Ca. As in the case of fcc Ca, there has been no direct experimental measurement of the elastic constants of bcc Ca, although Heiroth *et al.*, did obtain estimates for C_{44} and the tetragonal shear constant $[C'=\frac{1}{2}(C_{11}-C_{12})]$ by fitting the low-frequency region of their spectra. Since we require a complete set of elastic constants, we have adopted the values calculated by Singh and Singh[21] (S&S) who have performed seven shell effective-pair potential calculations using a modified Heine-Abarenkov model pseudopotential,[22] with parameters obtained by fitting the phonon frequency "data" of Heiroth *et al.* There is likewise no experimental or theoretical value available for the vacancy-formation energy of bcc Ca so the value of 0.5 eV, chosen for the fcc structure, has also been used for the bcc phase. The data used in the fitting procedure for bcc Ca are also summarized in Table I.

TABLE I. Data used in the optimization procedure. P_1-P_{14} and $P_{19}-P_{32}$ have been obtained from phonon frequencies $\omega(q)$: $P=M\omega^2(q)/r_1$, where M is the atomic mass (40.08) (Ref. 19) and r_1 the lattice constant (Ref. 2). These quantities have the same dimensions as the elastic constants $P_{15}-P_{17}$ and $P_{33}-P_{35}$ and are expressed in units of 10^{12} dyn cm^{-2}.

	Phonon vector	Mode	Value	
	fcc: $r_1=5.5884$ Å, $U=1.84$ eV (Ref. 20)			
P_1	0.5,0,0	L	0.6298	$P_{15}=C_{11}=0.2780$
P_2	0.5,0,0	T	0.3033	$P_{16}=C_{12}=0.1822$
P_3	1.0,0,0	L	0.9606	$P_{17}=C_{44}=0.1630$
P_4	1.0,0,0	T	0.6195	$P_{18}=E_{vac}=0.5$ eV
P_5	0.3,0.3,0.3	L	0.7151	
P_6	0.3,0.3,0.3	T	0.1540	
P_7	0.5,0.5,0.5	L	0.9992	
P_8	0.5,0.5,0.5	T	0.2619	
P_9	0.4,0.4,0	L	0.7299	
P_{10}	0.4,0.4,0	$T1$	0.1265	
P_{11}	0.4,0.4,0	$T2$	0.3982	
P_{12}	0.7,0.7,0	L	0.7674	
P_{13}	0.7,0.7,0	$T1$	0.4288	
P_{14}	0.7,0.7,0	$T2$	0.9061	
	bcc: $r_1=4.480$ Å, $U=1.84$ eV			
P_{19}	0.5,0,0	L	0.8469	$P_{33}=C_{11}=0.3170$
P_{20}	0.5,0,0	T	0.5636	$P_{34}=C_{12}=0.2340$
P_{21}	1.0,0,0	$L=T$	1.4662	$P_{35}=C_{44}=0.1870$
P_{22}	0.3,0.3,0.3	L	1.0346	$P_{36}=E_{vac}=0.5$ eV
P_{23}	0.3,0.3,0.3	T	0.2586	
P_{24}	0.5,0.5,0.5	$L=T$	0.6387	
P_{25}	0.7,0.7,0.7	L	0.3103	
P_{26}	0.7,0.7,0.7	T	1.0346	
P_{27}	0.3,0.3,0	L	0.9384	
P_{28}	0.3,0.3,0	$T1$	0.0710	
P_{29}	0.3,0.3,0	$T2$	0.3103	
P_{30}	0.5,0.5,0	L	1.3513	
P_{31}	0.5,0.5,0	$T1$	0.0991	
P_{32}	0.5,0.5,0	$T2$	0.5279	

IV. POTENTIAL OPTIMIZATION

A. Fitting fcc Ca

We first obtained a potential by fitting the data for fcc Ca alone. The two-body terms $V_{ij}^{(2)}$ were summed over all atoms j within a radius of three times the nearest-neighbor distance about an arbitrary central atom i. For the fcc structure this means that we are including up to tenth-neighbor interactions.[9,11] The three-body terms

TABLE II. Comparison of the best fcc, bcc, and dual-optimized potentials. A measure of the accuracy of the fit to data is given by the quantity $F = \frac{1}{n}\left[\sum_i [(P_i^{\text{calc}} - P_i^{\text{data}})/P_i^{\text{data}}]^2\right]^{1/2}$. Elastic constants in units 10^{12} dyn cm^{-2}. Asterisks show values either fixed or optimized to data.

	fcc	bcc	Dual	Data
F (fcc)	0.014	0.045	0.026	
F (bcc)	0.375	0.022	0.024	
C_{11} (fcc)	0.267*	0.296	0.309*	0.278[a],0.228[b]
C_{12} (fcc)	0.191*	0.230	0.198*	0.182[a],0.16[b]
C_{44} (fcc)	0.149*	0.134	0.143*	0.163[a],0.14[b]
C_{11} (bcc)	0.509	0.309*	0.295*	0.317[c]
C_{12} (bcc)	0.500	0.232*	0.246*	0.234[c]
C_{44} (bcc)	0.403	0.121*	0.120*	0.187[c],0.12[b]
U (fcc)/eV	1.840*	1.843	1.840*	1.840
U (bcc)/eV	1.844	1.840*	1.818	1.840 est
E_{vac} (fcc)/eV	0.500*	0.470	0.538*	0.500 est
E_{vac} (bcc)/eV	0.457	0.500*	0.461	0.500 est
r_1 (fcc)/Å	5.588*	5.617	5.588*	5.588
r_1 (bcc)/Å	4.495	4.480*	4.361	4.480

[a]Reference 4.
[b]Reference 5.
[c]Reference 21.

$V_{ijk}^{(3)}$ were likewise summed over all atoms j and k within the two-body cutoff radius around i. The lowest sum of squared deviations was obtained for $a_2=6.0$; $a_3=7.0$, with the experimental phonon-dispersion curves reproduced exactly and elastic constants fitted very well. This potential, however, gave an order of stability, hcp > bcc > fcc, which is clearly incompatible with experiment. Although the fcc potential gives the bcc structure as a local minimum, it leads to a considerable overestimation of the phonon frequencies and elastic constants of bcc Ca (see Table II). This can be seen from the bcc mean root squared deviation F, defined and listed in Table II, which is more than 30 times higher than that for the fcc structure.

B. Fitting bcc Ca

The above procedure has been applied to the bcc data. The three-times nearest-neighbor cutoff leads to inclusion of 11 shells for the bcc structure.[10,12] We again obtained an excellent fit to the experimental phonon frequencies, and good elastic constants, with the best fit being obtained for $a_2=a_3=6.0$. This potential gave the fcc and bcc structures almost equal lattice energies, with the hcp structure 0.02 eV less stable. When applied to fcc Ca, the mean root squared deviation F (see Table II) for the fcc data is three times worse than with the fcc-optimized potential, with the calculated frequency of the higher mode at [1,0,0] on the Brillouin zone (BZ) surface being particularly poor. However, the overall picture from this potential is quite good and suggested that a dual optimization, of both the fcc and bcc data together, could be achieved.

C. Dual optimization

The approach we adopted for dual optimization (i.e., optimizing to two structures simultaneously) was to calculate the scaling factors D and r_e so that the fcc cohesive energy and lattice spacing are reproduced exactly, to calculate the fcc phonon frequencies and elastic constants, and then to use the potential to calculate the cohesive energy and lattice spacing of the bcc structure. The bcc phonon frequencies and elastic constants were then calculated for this theoretical bcc structure. The vacancy-formation energy for fcc Ca was included in the data set for fitting, but the bcc vacancy energy, cohesive energy, and lattice spacing were allowed to vary freely to provide an independent test of the potential.

The best potential derived with the dual optimization procedure is listed in Table III. Although the two-body exponent ($a_2=6.2$) is close to those of the fcc and bcc potentials, the three-body exponent ($a_3=9.5$) is significantly larger. For a_3 in the range 5–7, it was possible to get a good fit to the experimental lattice-dynamical data of both fcc and bcc Ca, but these potentials were found to be unsatisfactory: collapsing at short range and/or giving the wrong stability order of solid structures. A thorough search in the space of the exponents a_2 and a_3 was carried out which revealed that the best potentials which simultaneously fit the experimental data of fcc and bcc Ca and which have sensible orderings of 3D, 2D, and 1D lattices, and do not collapse at short internuclear separations, have large a_3 values. The relationship between potentials optimized to single structures (bcc or fcc) and dual optimized potentials is currently being investigated for a number of metals.

The phonon-dispersion curves, calculated using the dual optimized potential of Table III, for fcc and bcc Ca, are shown in Figs. 1 and 2, respectively. The agreement with experiment is excellent, with the largest error being in the higher frequency mode at the point $[\frac{1}{2},\frac{1}{2},\frac{1}{2}]$ on the BZ surface. Our calculated frequencies are significantly better than those obtained by S&S (for both fcc and bcc Ca), using force constants calculated from their semiempirical pseudopotential.[21] They are also better than those obtained by Moriarty from his generalized pseudopotential calculations on fcc Ca,[6,23] and comparable with Wang and Overhauser's dynamic pseudopotential calculations on the fcc structure.[24] The fit is also better than

TABLE III. Dual-optimized potential function for Ca. Parameters are defined in expressions (1)–(5).

a_2	6.2	c_0	0.0476
a_3	9.5	c_1	1.1610
		c_2	6.5902
D/eV	0.399	c_3	0.2765
r_e/Å	4.012	c_4	2.8266
		c_5	−5.6875
		c_6	4.5711
		c_7	13.6829
		c_8	0.2587
		c_9	−14.2926
		c_{10}	19.9282

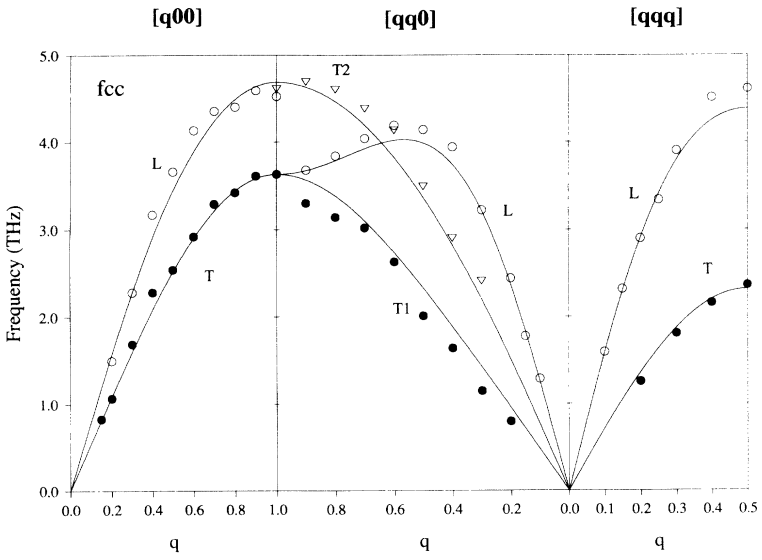

FIG. 1. Phonon-dispersion curves for fcc Ca along high-symmetry lines $[q00]$, $[qq0]$, and $[qqq]$. The solid lines have been calculated using the dual-optimized quartic potential listed in Table III. Experimental data (circles and triangles) have been taken from Stassis *et al.* (Ref. 4). L = longitudinal modes; T = transverse modes. The reduced wave vector **q** is in units of $2\pi/r_1$ (where r_1 is the lattice spacing).

that obtained by Li and Goddard, from their interstitial electron model.[25] In fact, for both the fcc and the bcc phases, our phonon-dispersion curves are effectively as good as the direct (unconstrained by an underlying potential) BvK fits to the experimental data performed by Stassis *et al.*,[4] Heiroth *et al.*,[5] and Ghorai.[18]

The elastic constants are fitted satisfactorily, given that there are no direct experimental measurements for either structure. Our calculated value for C_{44} (bcc) is significantly smaller than the value (due to S&S) (Ref. 21) used in our optimization, and is in fact equal to the value obtained by Heiroth *et al.* by fitting the low-frequency polycrystalline neutron data.[5]

Perhaps the most significant defect in our potential is that, as can be seen from Table II, we underestimate the value of the lattice spacing (r_1) for the bcc structure (we calculate a value of 4.361 Å, compared with the experimental value of 4.480 Å).[2] This makes the bcc structure more dense (volume per atom, $V_{bcc}=41.47$ Å^3) than fcc (volume per atom, $V_{fcc}=43.63$ Å^3), contrary to experiment (the experimental value of V_{bcc} is 44.96 Å^3),[2]. Possible reasons for this discrepancy include the neglect of anharmonicity (which may be large for bcc Ca at 726 K) and the fact that there is no explicit temperature dependence of the potential in our model.

It should be noted that the fcc-optimized potential leads to a bcc structure ($r_1=4.495$ Å; $V_{bcc}=45.41$ Å^3) which is less dense than fcc and the bcc-optimized potential gives an fcc structure ($r_1=5.617$ Å; $V_{fcc}=44.31$ Å^3) which is more dense than bcc, in agreement with experiment. Though neither of these potentials was a suitable candidate for a global Ca potential, for reasons which have been given above, we believe that it should be possible (without introducing anharmonicity or explicit temperature dependence into the potential) to obtain a dual-optimized potential which has the correct ordering of bcc

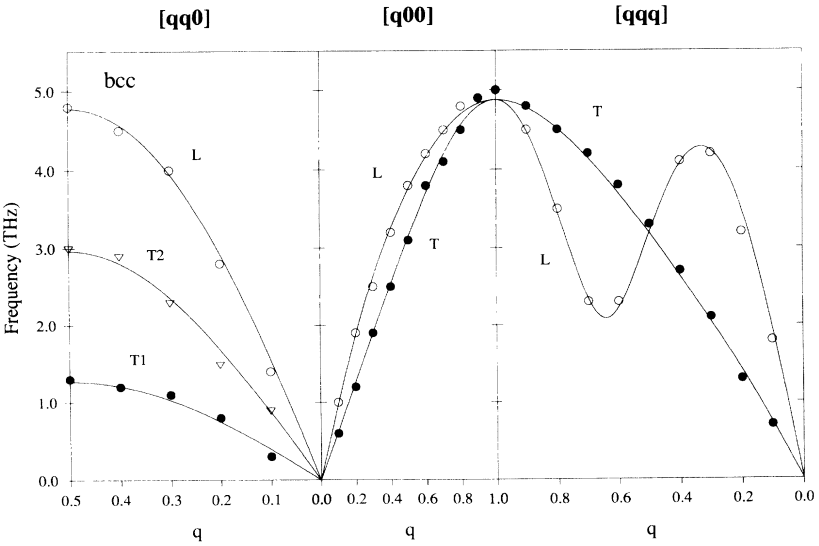

FIG. 2. Phonon-dispersion curves for bcc Ca along high-symmetry lines $[q00]$, $[qq0]$, and $[qqq]$. The solid lines have been calculated using the dual-optimized quartic potential listed in Table III. Experimental data (circles and triangles) have been taken from Heiroth *et al.* (Ref. 5). The reduced wave vector **q** is in units of $2\pi/r_1$ (where r_1 is the lattice spacing).

and fcc densities, by including the experimental lattice constant of bcc in the fitting procedure and this is currently being investigated.

V. APPLICATIONS OF THE DUAL-OPTIMIZED POTENTIAL

A. Relative stabilities of other solid structures

For a potential to be applicable to the study of the statics and dynamics of solids, surfaces, liquids, and clusters, it should be valid over a wide range of coordination numbers and geometries. We have therefore used our potential, which was optimized to the lattice-dynamical properties of fcc and bcc Ca to calculate the cohesive energies, nearest-neighbor distances, and vacancy-formation energies of a number of infinite 1D, 2D, and 3D structures.[9,27] The results of these calculations are listed in Table IV.

The bcc cohesive energy, which is not fitted in our optimization procedure, is calculated to be 0.022 eV smaller than that of fcc. This value for the difference in energy between the bcc and fcc structures is consistent with those calculated by Moriarty (0.005–0.024 eV) (Refs. 6 and 23) and Skriver, using the linear muffin-tin orbital method (0.024 eV).[26] The bcc lattice spacing (also not fitted) is calculated to be 0.119 Å shorter than the experimental high-temperature value of 4.48 Å.[2] Due to anharmonicity the lattice spacing increases with increasing temperature, so our underestimation is consistent with our potential having an effective temperature which is lower than that at which the lattice constant was measured.

The hcp structure is calculated to be approximately 0.001 eV less stable than fcc, consistent with the calculations of Moriarty[6,23] and Skriver,[26] who calculate a difference in cohesive energy ranging from −0.004 eV (i.e., hcp more stable than fcc) to 0.012 eV. The other structures show a general decrease in stability with decreasing coordination number, due to the dominance of the two-body potential-energy term.

TABLE IV. Calculated nearest-neighbor distances (d) and cohesive energies U for some 3D, 2D, and 1D structures. sh=simple hexagonal, dia=diamond, $f111$, $f100$, and $f110$ are 2D, two-layer slabs of atoms at the fcc surfaces specified. tri, sq, and hex are 2D single-layer planar nets of triangles, squares, and hexagons, respectively.

	Structure	Coord. No.	d (Å)	U (eV)
3D	fcc	12	3.95	1.840
	hcp	12	3.95	1.839
	bcc	8	3.78	1.818
	sh	8	3.90	1.61
	sc	6	3.47	1.49
	dia	4	3.06	1.47
2D	$f111$	9	3.92	1.53
	$f100$	8	3.90	1.45
	$f110$	6	3.91	1.18
	tri	6	3.96	1.11
	sq	4	3.91	0.88
	hex	3	3.97	0.62
1D	zig-zag	4	3.96	0.76
	linear	2	4.02	0.40

B. The Bain deformation

Since the dual-optimized potential gives both the fcc and bcc structures as local minima (i.e., both structures are mechanically stable), it is interesting to consider pathways which can interconvert these phases. In principle there are a large number of diffusionless (Martensitic) transformations which can accomplish this interconversion.[28] One such homogeneous strain pathway, involving minimum atomic motion, is the tetragonal Bain deformation;[29] this interconverts fcc and bcc via a body-centered tetragonal (bct) transition state. Figure 3 shows the correspondence between the bct cell (shaded atoms) and the larger face-centered-tetragonal (fct) cell (dotted lines), which is rotated by 45° with respect to the bct cell. In terms of the bct definition the bcc and fcc structures occur when the c/a ratio is 1.0 and $\sqrt{2}$, respectively. The fcc structure can therefore be smoothly transformed into bcc by contracting parallel to the c axis and expanding parallel to the a and b axes.

In calculating the cohesive energy of Ca along the Bain path we used a cutoff of three times the nearest-neighbor distance, as in the potential optimization procedure. For this it was necessary to include 258 atoms around the origin atom in the coordinate data base, since this ensures that all the atoms that are within the cutoff at both extremes of the distortion path (which we calculated from $c/a = 0.8$ to 1.6) are included.

Figure 4 shows a plot of the cohesive energy (U) as a function of the c/a ratio along the Bain path, using the dual-optimized potential listed in Table III. Two minima can clearly be seen, corresponding to the bcc (local minimum, i.e., metastable) and fcc (global minimum) structures. That there are only two distinct minima related by the tetragonal distortion, may be seen from Fig. 5,

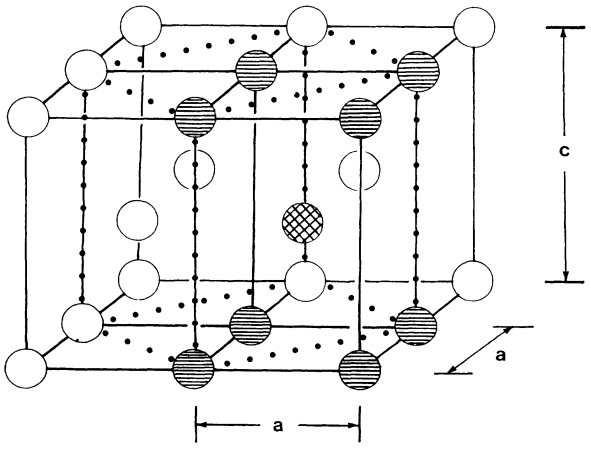

FIG. 3. Relationship between bct (shaded atoms) and rotated fct (dotted lines) unit cells. The body-centered atom of the bct cell is indicated by cross hatching.

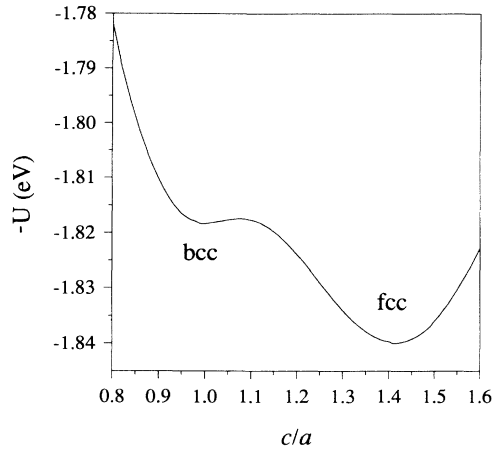

FIG. 4. Variation of cohesive energy (U) with c/a ratio along the Bain deformation path.

which is a contour map of the cohesive energy plotted against the reduced volume (V/V_0, where V_0 is the equilibrium atomic volume of the stable fcc phase; $V_0 = V_{\rm fcc} = 43.63$ Å^3) and the c/a ratio. *Ab initio* pseudopotential calculations by Morrison *et al.* on copper indicate a third minimum on the U vs $(V/V_0, c/a)$ surface, corresponding to a metastable bct phase,[29b] but we see no evidence for this. The above mentioned fact, that the dual-optimized potential makes the bcc structure more dense than fcc, shows up as $V_{\rm bcc}/V_0 < 1$.

For small deformations, the tetragonal shear elastic constant C' provides the restoring force against the Bain transformation for both the fcc and bcc structures.[5] The shear constant (which is related to the slope of the T_1 mode along $[qq0]$ at small values of q) (Refs. 5 and 12) is small for both phases [C' (fcc)=0.048 (Ref. 4); 0.034 (Ref. 5): C' (bcc)=0.016 (Ref. 5); 0.042 (Ref. 21): all values quoted are in units of 10^{12} dyn cm^{-2}]. Heiroth *et al.*, have argued[5] that, for fcc Ca, their value of C' is more accurate than that of Stassis *et al.*,[4] since the former was obtained by fitting to data obtained at lower q values. In the case of bcc Ca, the value of Heiroth *et al.* (directly fitted to experimental measurements) should be more reliable than that calculated by S&S (Ref. 21) from

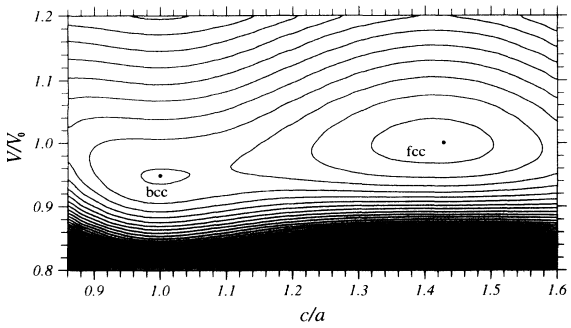

FIG. 5. Contour plot of the potential-energy surface for bct Ca as a function of c/a vs the reduced volume V/V_0. The contour spacing is 0.009 eV.

phonon-dispersion curves of Heiroth *et al.*

The values of C' for fcc and bcc Ca (Heiroth *et al.*) are consistent with a small energy difference between the two phases and a low activation barrier (and therefore low curvature of $E_{\rm coh}$ with displacement along the Bain path) for their interconversion. They also confirm the relative stability of fcc over bcc. Our calculations [Fig. 4(a)] indicate an activation barrier of ~ 0.023 eV for fcc$\rightarrow$bcc and ~ 0.001 eV for the reverse transformation; our calculated values for C' are 0.055×10^{12} dyn cm^{-2} (fcc) and 0.025×10^{12} dyn cm^{-2} (bcc).

C. Structures and stabilities of small Ca clusters

There is considerable current interest in the structures and properties of gas phase metal clusters, since they represent intermediates between discrete molecules and condensed matter.[30] *Ab initio* calculations by Lee, Rendell, and Taylor on Ca_3 and Ca_4 indicate singlet ground states with D_{3h} and T_d symmetries, respectively.[31] Martin *et al.* have produced mass spectroscopic evidence that large Ca clusters with up to 5000 atoms have structures based on icosahedral, rather than cuboctahedral (i.e., fcc-like) packing.[32]

In previous papers we have outlined an approach for using our empirical many-body potentials to optimize cluster geometries for a variety of elements.[9–12,15] In this

TABLE V. Binding energies per atom (E_b) of Ca_n clusters calculated from the potential of Table III. For $n \geq 8$ only the energy of the most stable structure is quoted. Those indicated (i) are saddle points with i imaginary vibration frequencies. Structures are shown in Fig. 6.

n	Structure	Symmetry	E_b (eV)
3	1	D_{3h}	0.39
	2	$D_{\infty h}$	0.27(2)
4	3	T_d	0.59
	4	D_{2h}	0.49(1)
5	5	D_{3h}	0.69
	6	C_{4v}	0.63(1)
6	7	O_h	0.77
	8	C_{2v}	0.76
	9	C_s	0.71(1)
	10	C_s	0.64(2)
7	11	D_{5h}	0.86
	12	C_{3v}	0.81
	13	C_2	0.81
8	14	C_s	0.89
9	15	C_s	0.95
10	16	C_s	0.99
11	17	C_s	1.03
12	18	C_s	1.08
13	19	I_h	1.14
14	20	C_s	1.13
15	21	C_s	1.15
16	22	C_1	1.16
17	23	C_1	1.17
18	24	C_1	1.20
19	25	D_{5h}	1.23
20	26	C_1	1.21

section we report the results of our calculations, using the dual-optimized potential of Table III, on small calcium clusters Ca_n ($n \leq 20$). Energy minimization is performed on precursors which are either fragments of the cubic solids and icosahedral structures or randomly generated structures. This procedure can give metastable structures (local minima) as well as the lowest energy structure, though we cannot guarantee that all minima (or even the global minimum) on the potential-energy surface have been found. Table V lists the structures and binding energies of the most stable cluster isometers that we have obtained for Ca_3-Ca_{20}, together with some metastable and transition state structures. The structures are shown in Fig. 6.

For Ca_3 and Ca_4 our potential predicts equilateral triangular (D_{3h}; 1) and tetrahedral (T_d; 3) structures, respectively, in agreement with the *ab initio* calculations of Lee, Rendell, and Taylor[31] Due to the closed-shell nature of the calcium atom, small clusters with high symmetries are closed-shell and do not undergo Jahn-Teller distortions, unlike small alkali metal clusters.[10] Table VI compares the bond lengths (r_b), binding energies (E_b) and vibrational frequencies (ω_i) of these two clusters, calculated from our potential, with those obtained by Lee, Rendell, and Taylor, together with our predictions for Ca_5 (trigonal bipyramidal geometry; D_{3h}; 5) and Ca_6 (octahedral; O_h; 7). Table VI shows that our potential leads to an overestimation of the stability (i.e., the binding energies are greater than those calculated by *ab initio* methods) of these small clusters, with a consequent underestimation of their bond lengths and overestimation of the vibrational frequencies. This probably reflects the fact that while the bonding in small Ca clusters is mainly due to van der Waals-type interactions, our potential, which was derived from the solid, has metallic-type bonding implicitly included via the parametrization procedure, which leads to stronger, shorter bonds than those due to dispersion forces. Table VI shows that, for our potential the bond lengths decrease from Ca_3 to Ca_6. This is consistent with the *ab initio* calculations on Ca_3 and Ca_4,[31] as well as previous calculations on small Be and Mg clusters,[33] and is the opposite trend to that observed for open-shell atoms.[9–11] It is not yet known at what nuclearity the average bond length starts to rise again towards the bulk value of 3.95 Å.

Table V reveals that the binding energy per atom (E_b) increases with increasing cluster nuclearity. This trend can be seen more clearly from Fig. 7, which is a plot of E_b vs n for Ca_n ($n = 2$–20). The rise is quite slow, so that for Ca_{20}, E_b is only 65% of the bulk value (1.84 eV). It

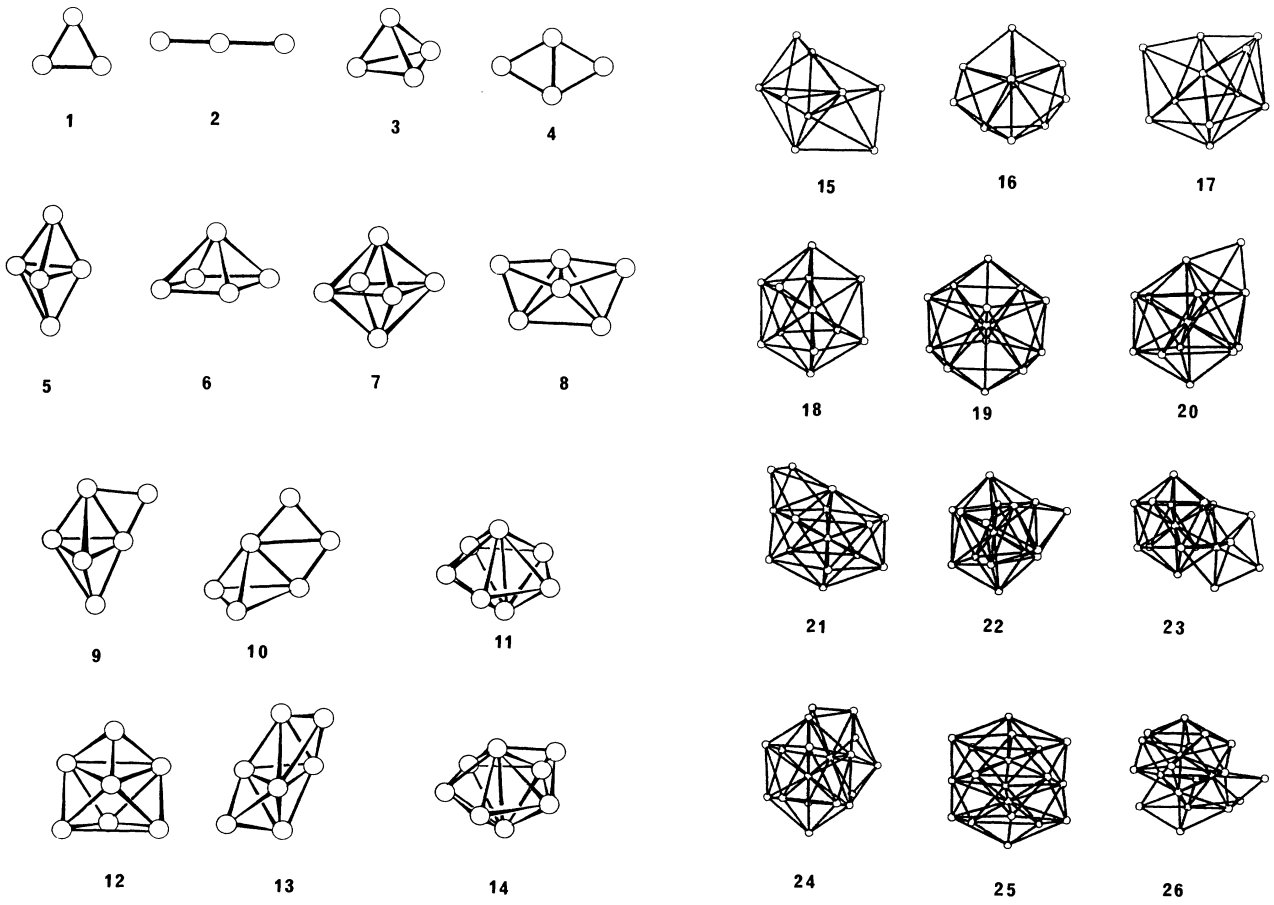

FIG. 6. Structures of the most stable clusters obtained, using the potential of Table III, for Ca_3-Ca_{20}. For Ca_3-Ca_7, some metastable and saddle point structures have also been included. The binding energies of these clusters are listed in Table V.

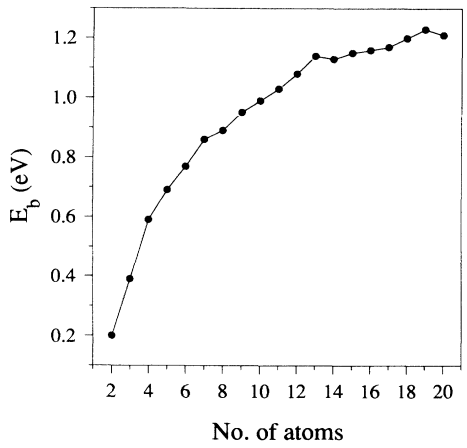

FIG. 7. Plot of binding energy per atom (E_b) against number of atoms for the most stable structures obtained, using the potential of Table III, for Ca_2-Ca_{20}.

can be seen from Fig. 6 that the most stable structures (that we have found) tend to be based on the fusing of tetrahedral units. Such "polytetrahedral" growth,[34] which maximizes atomic coordination, has previously been observed for alkali metal and noble-metal clusters and leads eventually, *via* building blocks such as the pentagonal bipyramid (the most stable geometry for Ca_7; **12**), to centered icosahedral Ca_{13} (I_h; **19**) and larger fused icosahedral structures such as Ca_{19} (D_{5h}; **25**). Kinks in the curve of E_b vs n at these "*magic number*" nuclearities (Ca_{13} and Ca_{19} actually have higher binding energies per atom than Ca_{14} and Ca_{20}, respectively) arise due to the enhanced stability of these structures in which even the surface atoms have fairly high coordination numbers. The occurrence of large Ca clusters with icosahedral shell structures has been suggested by the experiments of Martin *et al.*[32] Similar growth patterns are observed for inert gas clusters,[30] which are also closed-shell systems.

VI. CONCLUSIONS

In this paper we have shown that it is possible to derive a many-body potential for calcium by simultaneously fitting the lattice-dynamical properties of fcc and bcc Ca. This potential gives a very good fit to the experimental phonon frequencies and elastic constants of both structures. It also gives a reasonable stability ordering for a number of 1D, 2D, and 3D solids and a smooth, continuous reaction profile (along the Bain path) for the interconversion of the fcc and bcc structures. When applied to small Ca clusters the potential gives results (predicted geometries, bond lengths, binding energies and vibrational frequencies) which are in qualitative agreement with *ab initio* calculations.

In view of the successful application of the potential to a range of problems, we are satisfied that the search for a global calcium potential, i.e., one that will be valid over a wide range of structures and may, therefore be applied to study liquids, surfaces, large clusters, etc., is worthwhile and that the dual-optimized potential reported here represents a significant step towards that goal. The search for such a global potential would be aided by more accurate, directly measured elastic constants for both fcc and bcc Ca, as well as good estimates of the vacancy-formation energies of these structures.

TABLE VI. Calculated binding energies (per atom), bond lengths and vibration frequencies for small calcium clusters and comparison with best *ab initio* results (CCSD(*T*); 6*s* 5*p* 2*d* 1*f*; numbers in parentheses), (Ref. 31).

Cluster	E_b (eV)	r_b (Å)	ω_i (cm^{-1})
Ca_3(**1**)	0.39(0.16)	3.97(4.17)	106(83), 145(94)
Ca_4(**3**)	0.59(0.34)	3.93(4.02)	94(86), 132(105), 187(127)
Ca_5(**5**)	0.69	3.90, 3.93	73, 112, 124, 139, 167, 204
Ca_6(**7**)	0.77	3.92	75, 89, 125, 157, 179

ACKNOWLEDGMENTS

R.L.J. thanks the Royal Society for financial support. The authors are grateful to Dr. A. P. Rendell for copies of Refs. 31 and 33 and to Dr. B. R. Eggen, Dr. A. V. Nikolaev, and Dr. J. Uppenbrink for helpful discussions.

[1]J. Donohue, *The Structures of The Elements*, 2nd ed. (Wiley, New York, 1974).
[2]W. B. Pearson, *A Handbook of Lattice Spacings and Structures of Metals and Alloys* (Pergamon, New York, 1958).
[3]H. Olijnyk and W. B. Holzapfel, Phys. Lett. A **100**, 191 (1984); Phys. Rev. B **31**, 4682 (1985).
[4]C. Stassis, J. Zaretsky, D. K. Misemer, H. L. Skriver, B. N. Harmon, and R. M. Nicklow, Phys. Rev. B. **27**, 3303 (1983).
[5]M. Heiroth, U. Buchenau, H. R. Schober, and J. Evers, Phys. Rev. B **34**, 6681 (1986).
[6]J. A. Moriarty, Phys. Rev. B **34**, 6738 (1986).
[7]J. N. Murrell and R. E. Mottram, Mol. Phys. **69**, 571 (1990).
[8]J. N. Murrell and J. A. Rodriguez-Ruiz, Mol. Phys. **71**, 823 (1990).
[9]R. L. Johnston and J.-Y. Fang, J. Chem. Phys. **97**, 7809 (1992).
[10]J.-Y. Fang, R. L. Johnston, and J. N. Murrell, Mol. Phys. **78**, 1405 (1993).
[11]J.-Y. Fang, R. L. Johnston, and J. N. Murrell, J. Chem. Soc. Faraday Trans. **89**, 1659 (1993).
[12]F. Gao, R. L. Johnston, and J. N. Murrell, J. Phys. Chem. (to be published).
[13]A. R. Al-Derzi, R. L. Johnston, J. N. Murrell, and J. A. Rodriguez-Ruiz, Mol. Phys. **73**, 265 (1991).
[14]B. R. Eggen, R. L. Johnston, S. Li, and J. N. Murrell, Mol. Phys. **76**, 619 (1992).
[15]S. Li, R. L. Johnston, and J. N. Murrell, J. Chem. Soc. Fara-

day Trans. **88**, 1229 (1992).
[16]S. N. Vaidya and G. C. Kennedy, J. Phys. Chem. Solids **31**, 2329 (1970).
[17][K] M. Manninen, R. Nieminen, P. Hautojärvi, and J. Arponen, Phys. Rev. B **12**, 4012 (1975); [Al] H.-E. Schaefer, Phys. Status Solidi A **102**, 47 (1987). For a compilation of vacancy-formation energies, see: J. P. Perdew, Y. Wang, and E. Engel, Phys. Rev. Lett. **66**, 508 (1991).
[18]A. Ghorai, Phys. Status Solidi B **167**, 551 (1991).
[19]A. A. Radzig and B. M. Smirnov, *Reference Data on Atoms, Molecules and Ions* (Springer-Verlag, Berlin, 1985).
[20]C. Kittel, *Introduction to Solid State Physics,* 6th ed. (Wiley, New York, 1986).
[21]N. Singh and S. P. Singh, Phys. Status Solidi B **158**, 433 (1990).
[22]V. Heine and D. L. Weaire, in *Solid State Physics: Advances in Research and Applications,* edited by H. Ehrenreich (Academic, New York, 1970), Vol. 24, p. 249.
[23]J. A. Moriarty, Phys. Rev. B **16**, 2537 (1977); **26**, 1754 (1982).
[24]Y. R. Wang and A. W. Overhauser, Phys. Rev. B **35**, 497 (1987).
[25]M. Li and W. A. Goddard, J. Chem. Phys. **98**, 7995 (1993).
[26]H. L. Skriver, Phys. Rev. Lett. **49**, 1768 (1982); Phys. Rev. B **31**, 1909 (1985).
[27]I. J. Robertson, M. C. Payne, and V. Heine, Europhys. Lett. **15**, 301 (1991); I. J. Robertson, V. Heine, and M. C. Payne, Phys. Rev. Lett. **70**, 1944 (1993).
[28]D. A. Porter and K. E. Easterling, *Phase Transformations in Metals and Alloys,* 2nd ed. (Chapman and Hall, London, 1992).
[29](a) E. C. Bain, Trans. AIME **70**, 25 (1924). For recent theoretical studies of Bain transformations and related deformations, see: (b) [Cu] I. A. Morrison, M. H. Kang, and E. J. Mele, Phys. Rev. B **39**, 1575 (1989); (c) [Fe,Na] G. L. Krasko and G. B. Olson, *ibid.* **40**, 11 536 (1989); (d) [Al,Ir] M. J. Mehl and L. L. Boyer, *ibid.* **43**, 9498 (1991); (e) [Ag,Pt,Sr] K. Belay Seyoum, K. P. Thakur, and D. Jha, Phys. Status Solidi B **167**, 495 (1991).
[30]S. Sugano, in *Microcluster Physics,* edited by J. P. Toennies, Springer Series in Materials Science, Vol. 20 (Springer-Verlag, Berlin, 1991), and references therein.
[31]T. J. Lee, A. P. Rendell, and P. R. Taylor, Theor. Chim. Acta **83**, 165 (1992).
[32]T. P. Martin, U. Näher, T. Bergmann, H. Göhlich, and T. Lange, Chem. Phys. Lett. **183**, 119 (1991).
[33]T. J. Lee, A. P. Rendell, and P. R. Taylor, J. Chem. Phys. **92**, 489 (1990); A. P. Rendell, T. J. Lee, and P. R. Taylor, *ibid.* **92**, 7050 (1990); T. J. Lee, A. P. Rendell, and P. R. Taylor, *ibid.* **93**, 6636 (1990).
[34]D. R. Nelson and F. Spaepen, *Solid State Physics: Advances in Research and Applications,* edited by H. Ehrenreich (Academic, New York, 1989), Vol. 42, p. 1.